https://doi.org/10.5194/egusphere-2025-2631
Preprint. Discussion started: 29 July 2025

Modeling surface water and groundwater mixing and mixing-dependent denitrification with bedform dynamics

Xue Ping[1], Zhang Wen[1, 2*], Yang Xian[1], Menggui Jin[1, 2], Stefan Krause[3]

[1]Hubei Key Laboratory of Yangtze Catchment Environmental Aquatic Science, School of Environmental Studies, China University of Geosciences, Wuhan, China

[2]State Key Laboratory of Biogeology and Environmental Geology, China University of Geosciences, Wuhan, China

[3]School of Geography, Earth and Environmental Sciences, University of Birmingham, UK

*Corresponding author: Zhang Wen (wenz@cug.edu.cn)

https://doi.org/10.5194/egusphere-2025-2631
Preprint. Discussion started: 29 July 2025

Abstract The hyporheic zone (HZ), where surface water (SW) and groundwater (GW) interact and mix, acts as a critical interface that attenuates contaminants through enhanced biogeochemical cycling. While bedform migration significantly influences hyporheic exchange and non-mixing-driven reactions of solutes from upstream SW, the effects of bedform migration on SW-GW mixing dynamics and mixing-triggered biogeochemical reactions—particularly under gaining stream conditions—remain poorly understood. Pioneering a coupled hydrodynamic and reactive transport model that incorporates bedform migration this paper systematically examines nitrogen processing for scenarios of variable sediment grain size, stream velocities, and upwelling GW fluxes. Results of this study reveal that SW-GW mixing and mixing-triggered denitrification zones progressively transition from crescent shapes into uniform band-like configurations as bedforms migrate. Both hyporheic exchange flux and mixing flux increase with increasing stream velocity and associated bedform celerity. The mixing proportion and mixing zone size increase at the start of migration, while they remain approximately constant when turnover becomes the dominant water exchange mechanism for fine-medium sandy riverbed. Fast stream flows and migrating bedforms reduce solute residence timescales and limits denitrification opportunities. Consequently, nitrate removal efficiency from both stream- and groundwater-borne sources decreases significantly with bedform migration in fine-medium sandy sediments. The self-purification capacity of the HZ, and particularly its functioning as a natural barrier against GW contamination, is hindered under such dynamic bedform conditions. These findings highlight the need to maintain stable bedform conditions in restoration projects to enhance the capacity of HZ contaminant attenuation.

1. Introduction

https://doi.org/10.5194/egusphere-2025-2631
Preprint. Discussion started: 29 July 2025

Anthropogenic activities such as the intensification of agricultural practices with its increased used of mineral and organic fertilizers, together with high livestock densities and emissions of inadequately treated domestic and industrial wastewater have significantly increased nitrogen loading to rivers and groundwater, which impacts water quality, causing eutrophication, hypoxic and related deterioration of ecosystem functions (Conley et al., 2009; Rouse et al., 1999). Long-term regulatory monitoring data (e.g., from the UK) indicate that nitrate levels have stabilized in many rivers, while nitrate concentrations in groundwater-fed rivers continue to increase (Burt et al., 2011; Howden and Burt, 2008). The persistence of nitrate contamination in groundwater and associated risks of a "nitrate time bomb" (Ascott et al., 2019) has highlighted the urgency of exploring the potential of natural microbial processes to mediate nitrate transformation and removal in riverbed sediments (Shelley et al., 2017; Lansdown et al., 2015; Rivett et al., 2008).

The hyporheic zone (HZ) has received significant attention for its potential to facilitate enhanced nitrate transformation and removal via denitrification that is a primary process permanently reducing nitrate, with hyporheic exchange flows (HEFs) acting as a critical mechanism for transporting nitrate-rich surface water to the riverbed sediments where microbial activities and biogeochemical reaction rates are enhanced (Boano et al., 2014; Boulton et al., 1998; Cardenas, 2015; Xian et al., 2022; Krause et al., 2022). It has for long been assumed that predominantly stream waters provide inputs of bioavailable (mainly dissolved) organic carbon (DOC), oxygen (O_2) and nitrate (NO_3) into the riverbed where the residence and rection times determine the occurrence of aerobic respiration and the potential for shifts into anaerobic conditions that may facilitate denitrification along the HEF paths in the presence of enough remaining DOC (Zarnetske et al., 2011a, b). These hydrological and biogeochemical mechanisms are in this form mainly

https://doi.org/10.5194/egusphere-2025-2631
Preprint. Discussion started: 29 July 2025

representative of headwater streams, where the HEF is induced by stream flow turbulence (Boano et al., 2011; Roche et al., 2018, 2019), local geomorphological setting (Cardenas et al., 2008; Marzadri et al., 2012; Tonina and Buffington, 2007), and flow obstacles such as woody debris, streambed engineering or restoration structures (Briggs et al., 2013; Wondzell et al., 2009), and hyporheic nitrate removal processes expected to mainly occur at the middle to end- hyporheic flow paths within HEF cell sediments.

In lowland systems, groundwater-fed streams and rivers in permeable catchments will be dominated by base flow of often nitrate enriched groundwaters. The subsurface hydrological conditions are driven by horizontal HEF as well as vertical fluxes resulting from regional groundwater flow toward (or from) the stream. Spatial variability in regional groundwater flow can significantly affect hyporheic exchange and biogeochemical cycling (Boano et al., 2013; Krause et al., 2013; Munz et al., 2011; Naranjo et al., 2015). It is important to note that the groundwaters of many piedmont plains and lowlands are often contaminated with high nitrate concentrations, but usually low in bio-available DOC (Krause et al., 2022). When nitrate-rich groundwater upwells through deeper sediments and reaches a region enriched in availability of DOC, nitrate reduction processes are significantly facilitated in the condition (Krause et al., 2009; Naranjo et al., 2015; Ping et al., 2023; Trauth et al., 2017). Stelzer and Bartsch (2012) developed such a conceptual framework of nitrate-rich gaining fluvial setting from 8 sites in the Waupaca River Watershed with three order magnitude in groundwater nitrate concentration. Lansdown et al. (2014) also measured high denitrification rate at deep sediment in the coarse-grained sediments typical of groundwater-fed system, located within the River Leith (Cumbria, UK) where diverse nitrogen concentration changes were confirmed earlier (Krause et al., 2009).

https://doi.org/10.5194/egusphere-2025-2631
Preprint. Discussion started: 29 July 2025

Turnover and removal of the large amounts of NO_3^- from groundwater require DOC either from autochthonous streambed sources or from downwelling surface water to stimulate nitrate reduction (Krause et al., 2013, 2022; Ping et al., 2023; Sawyer, 2015; Trauth et al., 2017). For coarse grain or sandy riverbeds with low autochthonous organic matter content, stream-borne DOC dominates the supply of carbon sources for nitrogen transformation processes. Sandy sediments with less autochthonous organic carbon sources covering the majority of alluvial riverbeds are commonly characterized by topographical features such as ripples, dunes, and riffle-pool sequenced. The typical and multiple HEF cells induced by bedform topography are generally in crescent shapes (Fox et al., 2014; Wu et al., 2024). The downward advection of stream borne DOC provides electron donor and mixes with nitrate-rich and anoxic groundwater. It has been shown that the highest potential for mixing triggered denitrification is often found at the margin of the HEF cells, which represents the last natural protection before nitrate enter a stream (Hester et al., 2013, 2014; Gu et al., 2008; Nogueira et al., 2022).

The effects of mixing triggered denitrification on groundwater borne nitrate transformation in HZs have been studied almost exclusively for the case of stationary, that is immobile bedforms (Hester et al., 2017, 2019; Trauth and Fleckenstein et al., 2017; Ping et al., 2023). Bedforms are mobile in dynamic equilibrium or undergo constant changes during periods of moderate to high stream flow, and they are typically found in medium and larger waterways under realistic field conditions (Bartholdy et al., 2015; Risse-Buhl et al., 2023; Schindler et al., 2015). For example, Harvey et al. (2012) observed the migrating bedforms of dunes (with a median grain size D_{50} of 380 μm) at a velocity of 57.6 cm/h during base flow in the “Clear Run” stream in eastern North Carolina, USA. Ahmerkamp et al. (2017) found that the ripple bedforms for sands (D_{50} = 63 μm) ranged from

https://doi.org/10.5194/egusphere-2025-2631
Preprint. Discussion started: 29 July 2025

11 to 29 cm with a constant ratio of bedform height and length at 1/9, and migrated at velocities of 0.7–6.5 cm/h in the German Bight, Southeastern part of the North Sea. Bedforms migration complicates the development of hyporheic flow fields, increases solute exchange, alters redox conditions in riverbeds, and affects contaminant transport and transformation (Ahmerkamp et al., 2015; Schulz et al., 2023; Peleg et al., 2024). Specifically, bedform migration has negative influences on non-mixing-dependent denitrification (where nitrate and DOC are both derived from surface water and travel together along the flow paths) rate and nitrate removal efficiency (Jiang et al., 2022; Kessler et al., 2015; Ping et al., 2022; Zheng et al., 2019). However, no studies have yet investigated and explored the effects of bedforms migration on mixing of surface water and groundwater, as well as its controls and implications for mixing triggered denitrification reaction in groundwater-fed streams and rivers.

In this study, numerical modeling of hyporheic flow and multi-component solute transport is used to study the effect of bedform migration on mixing-dependent denitrification in the HZ of a gaining river, where the overlying water is induced into the sediment by ripple-type bedforms. The objectives of this study are to determine the effects of bedform migration on the overall extent and magnitude of mixing of surface water and upwelling groundwater, as well as its influences on groundwater borne nitrate transport and transformation.

2. Methods

2.1 Model description

Hyporheic flow, solute transport, and biogeochemical reactions were modelled in saturated sediments beneath a riverbed. Ripples form in the riverbed and migrate downstream due to sediment

https://doi.org/10.5194/egusphere-2025-2631
Preprint. Discussion started: 29 July 2025

bedload transport processes. The stream geometry is parameterized through its slope S, average water depth H, and mean velocity U. Triangular shaped ripple bedforms of wavelength λ are considered to develop and migrate downstream by a unidirectional average velocity u_c. Flow is driven by pumping (pressure variation along the bedform surface) and bedform migration processes and influenced by upwelling groundwater.

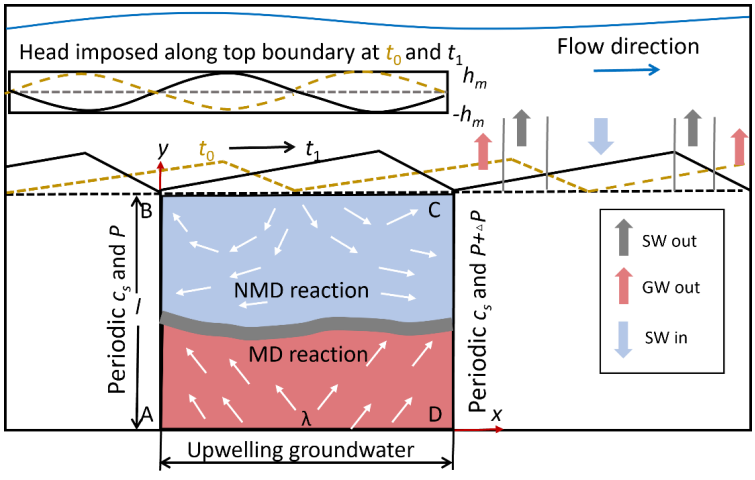

Figure 1. Schematic of the model domain with bed form geometry and boundary conditions. Stream flow and bedform migration are from left to right. The dashed yellow lines represent the streambed surface and head profile at time t_0, and the solid black lines represent the streambed surface and head profile after migration at t_1. "SW in" is where surface water enters the riverbed, and "SW out" is where surface water discharges to the stream, and "GW out" is along the upstream and downstream sides of bedforms where groundwater discharges to the stream. The gray band represents the mixing zone of surface water and groundwater. NMD reaction=non-mixing-dependent reaction and MD reaction=mixing-dependent reaction.

As bed migration occurs, sediment erosion and deposition primarily take place in the surface

https://doi.org/10.5194/egusphere-2025-2631
Preprint. Discussion started: 29 July 2025

layer of the streambed, thereby leading to the formation of bedforms such as ripples and dunes. In contrast, sediments in the deeper streambed layers remain relatively stable (Harvey et al., 2012; Precht et al., 2004). As illustrated in Figure 1, from the perspective of an observer stationary at a target riverbed segment with horizontal length λ, bedforms and their associated pressure fields migrate downstream at velocity u_c over the deeper immobile sediments (Ping et al., 2022; Teitelbaum et al., 2022). Given that ripple heights are negligible compared to the depth of the stable sediment domain, the undulating riverbed can be reasonably approximated as a flat bed with time-varying pressure patterns during bedform migration. Given the periodic nature of the morphological feature, we only focused on a representative section and constructed a two-dimensional rectangular domain of length 0.2 m and depth 0.16 m for modeling.

2.2 Model formulation

The pore water flow was calculated using Darcy's law and the groundwater flow equation:

$$\nabla \cdot \left(-K \nabla h\right) = 0 \tag{1}$$

where h [L] is the hydraulic head, and K [L T^{-1}] is the hydraulic conductivity.

The head profile on the streambed surface (BC) was described as a sinusoidal function that moves downstream by the ripple's migration velocity u_c (Ping et al., 2022):

$$h\big|_{y=l} = h_m \cdot \sin m(x - u_c dt) \tag{2}$$

where h_m [L] is the amplitude of the head variation, m [-] is the wave number of the variation ($m = 2\pi/\lambda$), the head difference is related to the properties of the overlying flow (Elliott and Brooks, 1997):

$$h_m = a \frac{U^2}{2g} \left(\frac{H_d / H}{0.34} \right)^n \tag{3}$$

https://doi.org/10.5194/egusphere-2025-2631
Preprint. Discussion started: 29 July 2025

where a = 0.28 [-] is a dimensionless coefficient, U [L T^{-1}] is the average stream velocity, H_d [L] is the height of the ripple, H [L] is the water depth, and g [L T^{-2}] is the gravity acceleration. The exponent n equals to 3/8 if $H_d < 0.34H$ and 3/2 otherwise.

The transport of reactive solutes within the streambed sediment was described by the advection-dispersion-reaction equation:

$$\frac{\partial c_i}{\partial t} - \nabla \cdot \left(\boldsymbol{D_{ij}} \nabla c_i \right) + \nabla \boldsymbol{v} \cdot c_i = R_i \tag{4}$$

where c_i [M L^{-3}] represents the concentration of reactive components, $\boldsymbol{v}$ [L T^{-1}] is the seepage or linear pore water velocity, $\boldsymbol{D_{ij}}$ [L^2 T^{-1}] is the hydrodynamic dispersion and is defined by Bear and Verruijt (1998):

$$\boldsymbol{D_{ij}} = \left(\alpha_L - \alpha_T \right) \cdot \frac{v_i v_j}{|v|} + \delta_{ij} \cdot \left(\alpha_T |v| + \theta \cdot \imath D_m \right) \tag{5}$$

where α_L [L] and α_T [L] are longitudinal and transverse dispersivities, respectively, D_m [L^2 T^{-1}] is molecular diffusion coefficient and $\imath$ [-] is tortuosity.

The reactive transport model considered three chemical species: DOC, O_2, and NO_3^-. In order to distinguish non-mixing-dependent and mixing-dependent denitrification, we divided nitrate into two separate pools, denoted s-NO_3^- for nitrate transported from the surface water and g-NO_3^- for nitrate from upwelling groundwater. The biogeochemical reactions are aerobic respiration (AR), non-mixing-dependent, and mixing-dependent denitrification (DN):

$$AR: CH_2O + O_2 \rightarrow CO_2 + H_2O \tag{R1}$$

$$DN: CH_2O + 0.8NO_3^- + 0.8H^+ \rightarrow CO_2 + 1.4H_2O + 0.4N_2 \tag{R2}$$

https://doi.org/10.5194/egusphere-2025-2631
Preprint. Discussion started: 29 July 2025

Reaction rates were defined using Monod kinetics (Zarnetske et al., 2012):

$$R_{AR} = V_{AR} \times X_{AR} \times \frac{c_{O_2}}{c_{O_2} + K_{O_2}} \times \frac{c_{DOC}}{c_{DOC} + K_{DOC}} \quad (6)$$

$$R_{DN} = V_{DN} \times X_{DN} \times \frac{c_{s/g-NO_3^-}}{c_{s/g-NO_3^-} + K_{NO_3^-}} \times \frac{c_{DOC}}{c_{DOC} + K_{DOC}} \frac{K_{inh}}{K_{inh} + c_{O_2}} \quad (7)$$

The reaction terms R_i was given by

$$R_{s-NO_3^-} = -R_{DN}(c_{s-NO_3^-}) \quad (8)$$

$$R_{g-NO_3^-} = -R_{DN}(c_{g-NO_3^-}) \quad (9)$$

$$R_{O_2} = -R_{AR} \quad (10)$$

$$R_{DOC} = -R_{AR} - 0.8(R_{DN}(c_{s-NO_3^-}) + R_{DN}(c_{g-NO_3^-})) \quad (11)$$

where V_{AR} and V_{DN} [T^{-1}] are the maximum reaction rate of aerobic respiration and denitrification, X_{AR} and X_{DN} [$M\ L^{-3}$] are the biomass of functional microbial groups facilitating the reaction components of AR and DN. K_{inh} [$M\ L^{-3}$] is a non-competitive inhibition factor used for representing inhibition of DN given oxygen availability.

The lateral boundaries AB and DC were set to be periodic boundaries: $P(0, y, t) = P(\lambda, y, t) + \Delta P$, $c_i(0, y, t) = c_i(\lambda, y, t)$ and $\partial c_i(0, y, t)/\partial y = \partial c_i(\lambda, y, t)/\partial y$. The additional pressure drop ΔP [$M\ L^{-1}T^{-2}$] is derived from the streambed gradient and calculated using $\Delta P = S\rho g\lambda$. The top boundary BC was specified as an open Dirichlet boundary with constant solute concentrations in the stream. An upward groundwater flux with constant nitrate concentration was specified at the bottom boundary AD to mimic a nitrate polluted groundwater discharge.

https://doi.org/10.5194/egusphere-2025-2631
Preprint. Discussion started: 29 July 2025

2.3 Bedform migration

The mechanisms of bedform initialization, formation and migration are initiated through a set of criteria to ensure that ripples are expected to form under the modeled scenarios and reach a state of dynamic equilibrium, where the ripples remain mobile while maintaining their shape. The development of ripples is assessed under different conditions of median particle size D_{50} and flow velocity based on a set of quantitative criteria (as reference in Ping et al., 2022 for criteria on ripple formation). For a specific grain size of streambed sediment, particular stream velocities that fulfill all these criteria for the development of ripple bedforms that are mobile under dynamic equilibrium are selected (Figure 2). All simulation scenarios were listed in the Table S3 in the supplementary material.

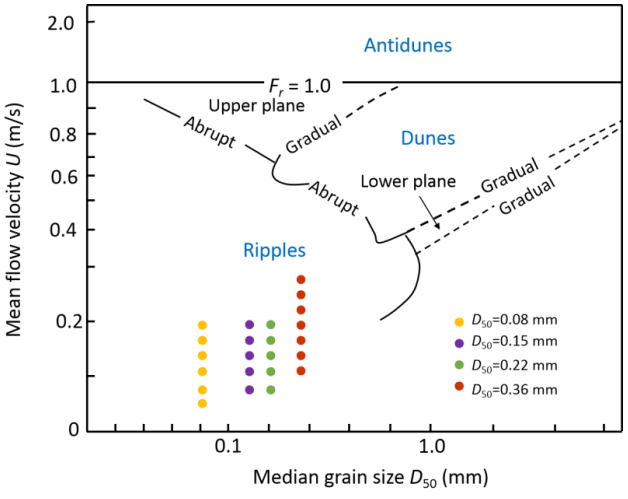

Figure 2. The bedform stability diagram (modified from Ashley, 1990) showing the bedform properties and hydraulic conditions considered in this study.

Ripple migration velocities are implemented using an empirical relation after Coleman and Melville (1994), which was derived from flume experiments:

https://doi.org/10.5194/egusphere-2025-2631
Preprint. Discussion started: 29 July 2025

$$\frac{u_c}{\left(u^* - u_{cr}^*\right)\left(\tau^* - \tau_{cr}^*\right)}\left(H_d / D_{50} - 3.5\right)^{1.3} = 40 \quad (12)$$

where D_{50} [L] is the median grain size, $u^* = (gHS)^{0.5}$ [L T^{-1}] is the bed shear velocity, S [-] is the stream gradient and calculated by Chezy equation ($U = H^{2/3}S^{1/2}/n$, where n [-] is the Manning coefficient and assumed to be 0.02 for sand). u_{cr}^* [L T^{-1}] is the critical bed shear velocity and it can be calculated by the critical Shield parameter τ_{cr}^* ($\tau_{cr}^* = \tau_{cr} / g(\rho_s - \rho)D_{50}$, $u_{cr}^* = (\tau_{cr} / \rho)^{0.5}$, ρ_s [M L^{-3}] and ρ [M L^{-3}] are the density of sediment and water), and τ^* is the shield number related to the bed shear velocity ($\tau^* = u^{*2}/rgD_{50}$). The critical shields parameter defines the threshold for the initialization of motion. The derived celerity was substituted into Equation (2) to determine the migration of sinusoidal head profile with ripples moving.

2.4 Governing non-dimensional numbers

The characteristics of the modeled system were depicted by a series of non-dimensional numbers, which represent the relative dominance of various forces, transport, and reaction processes in this system. Firstly, we used the Reynolds number Re to characterize the flow condition of surface water (Cardenas and Wilson, 2006):

$$Re = \frac{UH_d}{\upsilon} \quad (13)$$

where υ [L^2 T^{-1}] represents kinematic viscosity of water.

We introduced the dimensionless parameter U_r [-] to represent the relative magnitude of bedform celerity and the pressure-induced pore water velocity driven by pressure variation over the ripple surface and upwelling groundwater:

https://doi.org/10.5194/egusphere-2025-2631
Preprint. Discussion started: 29 July 2025

$$U_r = \frac{\theta \cdot u_c - u_s}{u_p} \tag{14}$$

where u_s [L T^{-1}] is the seepage velocity of the underflow induced by stream gradient ($u_s = KS$), and thus the characteristic horizontal velocity is $u_c - u_s/\theta$. u_p/θ [L T^{-1}] is the pore water velocity induced by pumping process and is calculated using the analytical solution after Boano et al. (2009) and Fox et al. (2014) accounting for vertical groundwater flux (u_q):

$$u_p = u_{p,0}\sqrt{1-\left(u_q/\pi u_{p,0}\right)^2} + \left(\left|u_q\right|/\pi\right)\sin^{-1}\left(\left|u_q\right|/\pi u_{p,0}\right) - \left(\left|u_q\right|/2\right) \tag{15}$$

$$u_{p,0} = a\frac{KU^2}{g\lambda}\left(\frac{H_d/H}{0.34}\right)^m \tag{16}$$

where $u_{p,0}$ represents the hyporheic exchange driven by pressure variation over the sediment-water interface; if $U_r > 1$, turnover process dominates and controls the hyporheic exchange, otherwise, the system is pumping process dominated (Jiang et al., 2022).

The relative magnitude of hyporheic exchange flux driven by pressure variation along the ripple surface and upwelling groundwater flux is determined as:

$$U_b = \frac{u_q}{u_{p,0}} \tag{17}$$

The relative dominance of hyporheic exchange and biogeochemical reaction in nitrate removal can be defined by the Damköhler number (Ocampo et al., 2006; Zarnetske et al., 2012; Zheng et al., 2019):

$$Da = \frac{\tau_T}{\tau_R} \tag{18}$$

the characteristic timescale for the transport of solutes through the ripple is estimated as (Azizian et

https://doi.org/10.5194/egusphere-2025-2631
Preprint. Discussion started: 29 July 2025

al., 2015):

$$\tau_T = \frac{\lambda\theta}{\pi^2 u_p} \quad (19)$$

and the reaction timescale τ_R represents the time needed to consume dissolved oxygen of hyporheic water to a prescribed anoxic environment threshold (2 mg/L). The reaction timescale is described as:

$$\tau_R = \frac{\ln\left(c_{O_2}/c_{O_2,\mathrm{lim}}\right)}{V_{AR}} \quad (20)$$

biogeochemical reactions are transport-limited when $Da < 1$. The biogeochemical reactions depended on reaction kinetics due to the brevity of the time that reactants spend within the HZ. Under these low Da conditions, the HZ remains oxic conditions, resulting in a minimal or no denitrification to occur. Conversely, when $Da > 1$, the residence time of reactants exceeds the reaction time, and thus oxygen is consumed and favors for the occurrence of denitrification in anoxic conditions (Jiang et al., 2022; Zarnetske et al., 2011a).

2.5 Model setup and parametrization

All parameter values in this study were shown in Table 1. The bedform geometry of Ping et al. (2022) was adopted for this study (streambed length and height: λ = 0.2 m and l = 0.16 m; the ripples located at λ_c = 0.15 m with a height of H_d = 0.02 m). Here grain sizes D_{50} of 0.08, 0.15, 0.22 and 0.36 mm were considered, typically falling within characteristic grain diameters on sandy riverbeds (Ahmerkamp et al., 2017; Harvey et al., 2012). We used the empirical relation $k = Da \times 735 \times 10^6 \times D_{50}^2$ (where $Da = 9.869 \times 10^{-13}$ is the conversion factor for unit Darcy to m^2; Gangi, 1985).

The concentrations of DOC, O_2, and s-NO_3^- in stream were specified as 30 mg/L, 8 mg/L, and 5 mg/L. This configuration represents a pristine stream characterized by moderate nutrient levels

https://doi.org/10.5194/egusphere-2025-2631
Preprint. Discussion started: 29 July 2025

(Ocampo et al., 2006). The g-NO_3^- in groundwater was set as 15 mg/L, representing the chemical signature of nitrate-contaminated groundwater that lacks both oxygen and organic matter (Hester et al., 2014). The maximum reaction rate and corresponding functional microbial concentration for AR and DN are listed in Table 1, the choose biogeochemical values are consistent with the parameter setting of nutrient cycling in hyporheic zones and riparian zones (Gu et al., 2008; Nogueira et al., 2021; Zarnetske et al., 2012).

Table 1. Model parameters used in numerical simulations

Parameter	Description	Value
l [m]	Streambed depth	0.16 [a, b]
l_c [m]	Ripple crest	0.15 [a, b]
λ [m]	Wavelength of ripple	0.2 [a, b]
H_d [m]	Height of ripple	0.02 [a, b]
H [m]	Stream water depth	0.1 [a, b]
θ [1]	Porosity	0.38
α_L [m]	Longitudinal dispersivity	0.01
α_T [m]	Transverse dispersivity	0.001
K_{inh} [mg L^{-1}]	Inhibition constant	0.25 [c, d]
K_{DOC} [mg L^{-1}]	Half-saturation constant for dissolved organic carbon	6 [c, d]
K_{NO3} [mg L^{-1}]	Half-saturation constant for nitrate	1 [c, d]
K_{O2} [mg L^{-1}]	Half-saturation constant for dissolved oxygen	0.5
V_{DN} [h^{-1}]	Maximum specific uptake rate for denitrification	1 [c, d]
V_{AR} [h^{-1}]	Maximum specific uptake rate for aerobic respiration	2 [c, d]

https://doi.org/10.5194/egusphere-2025-2631
Preprint. Discussion started: 29 July 2025

C_{DOC} [mg L^{-1}]	Concentration of dissolved organic carbon in stream	30
C_{O2} [mg L^{-1}]	Concentration of dissolved oxygen in stream	8
$C_{s\text{-}NO3^-}$ [mg L^{-1}]	Concentration of nitrate in stream	5
$C_{g\text{-}NO3^-}$ [mg L^{-1}]	Concentration of nitrate in groundwater	15

[a] Janssen et al. (2012) [b] Ping et al. (2022) [c] Zarnetske et al. (2012) [d] Sawyer (2015)

The following distinct model experiments were carried out: The Reynolds number, i.e., mean stream velocity, was varied for Re = 2000–6000 in intervals of 500, with corresponding stream water velocities of U = 0.1–0.3 m/s. The range of U_b was set from 0.3 to 0.7 in intervals of 0.1. A larger upward flux than $0.9\times u_{p,0}$ would eliminate the entire hyporheic flow cell, thus we set the maximum boundary flux at a value slightly below this threshold. Meanwhile a minimum of $0.2\times u_{p,0}$ ensures that upwelling groundwater is still mixing with surface water with minor influences on hyporheic flow cell.

The finite element software, COMSOL Multiphysics (version 6.1) was used to solve the Darcy flow and multi-component solute transport model. The domain was discretized with a grid spacing from 4×10^{-4} to 0.2 cm, the resultant mesh consisting of 19,940 elements. To maintain a constant bedform displacement (Δx) per timestep, the simulation was conducted with Δx = 2 cm, while dt was adjusted in inverse proportion to the migration celerity u_c. The total duration of the simulation was set to be equal to the time needed for hundreds of ripples to travel across the modeled domain until the hyporheic exchange and biogeochemical processes reached quasi-steady states.

2.6 Model Metrics

2.6.1 Mixing of surface water and groundwater

https://doi.org/10.5194/egusphere-2025-2631
Preprint. Discussion started: 29 July 2025

Mixing occurs at the interface between regions of advected surface water and upwelling groundwater, where the flow paths from these two sources run parallel to each other. We specified a constant concentration of conservative tracer (c_{gw} = 1 mg/L) in groundwater to represent groundwater. The tracer plume is used to visualize the surface water and groundwater mixing size and calculate the mixing magnitude quantitatively. The mixing zone is defined as the area where the groundwater proportion varies between 16% and 84% (Santizo et al., 2020). The size of the surface water and groundwater mixing zone (A_{mix}) was calculated by integrating the area where the concentration of the conservative tracer ranges from 0.16 to 0.84 mg/L.

The amount of tracer mass that undergoes mixing as it transitions from flow paths originating at the bottom boundary to those emerging at the streambed surface was quantified to determine the net effect of mixing occurring along the entire length of the mixing zone. The streambed surface was divided into three zones (Figure 1): “SW IN”, where surface water enters the bed; “SW OUT”, where surface water discharges back into the overlying water column; and “GW OUT”, where upwelling groundwater discharges into the stream. The mass flux for the SW OUT zone was used to describe mixing. If no mixing occurred, all the conservative tracer mass entering the model at the bottom boundary would exit through the GW OUT zone on the streambed surface. The mixing flux (MF) across the sediment-water interface was determined by integrating the Darcy flux flowing outward through the SW OUT zone, representing the total cumulative effect of mixing along the entire length of the mixing zone (Hester et al., 2013).

2.6.2 Nitrate reaction rate and efficiency

When the hydro-physical and biogeochemical conditions reach a quasi-steady state, we select

https://doi.org/10.5194/egusphere-2025-2631
Preprint. Discussion started: 29 July 2025

the last 10 periods of ripple migration and calculate the total amount of stream- or groundwater-borne nitrate being induced into the riverbed during the time interval:

$$M_{in,s-NO_3^-} = B\int_{\Delta T} c_{s-NO_3^-} F_{SWI} dL_{top} dT \quad (21)$$

$$M_{in,g-NO_3^-} = B\int_{\Delta T} c_{g-NO_3^-} q dL_{bottom} dT \quad (22)$$

where B [L] is the per unit width, F_{SWI} [L T^{-1}] is the inward flux across the ripple surface.

The total amount of nitrate removed by non-mixing-dependent (NMD) denitrification and mixing-dependent (MD) denitrification are calculated as follows during the same time interval:

$$M_{NMD} = B\int_{\Delta T}\int R_{DN}(c_{s-NO_3^-}) dA dT \quad (23)$$

$$M_{MD} = B\int_{\Delta T}\int R_{DN}(c_{g-NO_3^-}) dA dT \quad (24)$$

where A [L^2] is the area of the streambed.

The nitrate removal efficiency is defined as the ratio of the amount of nitrate being removed by DN to the amount of nitrate being induced into the riverbed:

$$N_{RE-NMD} = \frac{M_{NMD}}{M_{in,s-NO_3^-}}, \quad N_{RE-MD} = \frac{M_{MD}}{M_{in,g-NO_3^-}} \quad (25)$$

3. Results

3.1 Model validation

The model development was validated by comparison to flume experiments of Wolke et al. (2019) that were conducted to study the evolution of oxygen in the riverbed under different conditions of mean stream velocity (0.16−0.32 m/s) and bedform migration celerity (0−0.394 cm/h). No upwelling flux of groundwater was considered at the bottom of the riverbed. The experiment was

https://doi.org/10.5194/egusphere-2025-2631
Preprint. Discussion started: 29 July 2025

designed with a total of 5 operating conditions, each of which was repeated twice and labeled as Set 1 and Set 2. Based on the criteria for ripple migration, it was determined that under the hydraulic conditions of Run 5, ripples could not migrate while maintaining their shapes due to increased flow intensity. Therefore, the model validation simulations considered four hydraulic conditions of Run 1 to 4.

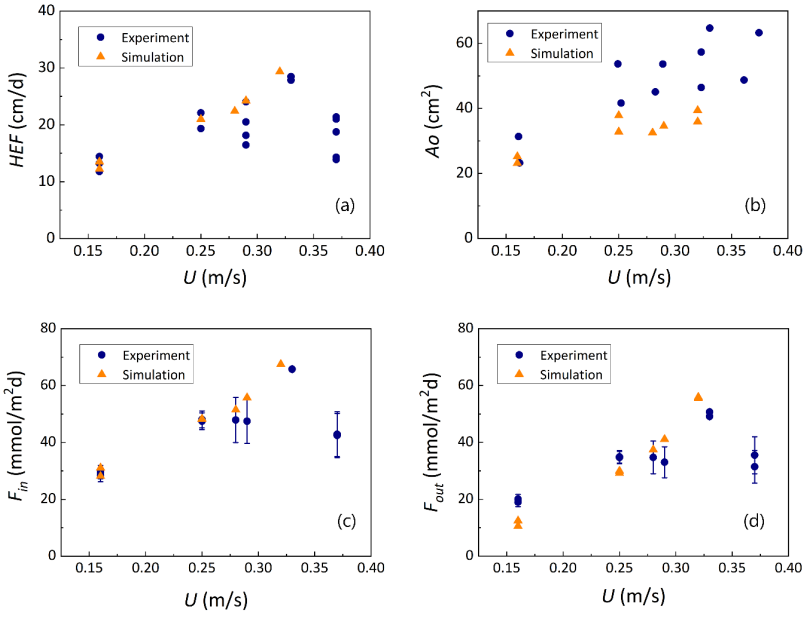

Figure 3. Comparison of numerical modeled (a) hyporheic exchange flux, (b) summed oxic zone and (c) oxygen influx and (d) oxygoutflux and experimental measurements by Wolke et al. (2019) under various conditions.

The parameters used for model validation are shown in supporting information Table S1 and S2. In stationary and slow-migrated beds, the spatial distribution of oxygen creates a typical conchoidally-shaped plume in the riverbed. In contrast, for fast-migrated beds, the oxygen plume becomes a more uniform front (Ping et al., 2022). The comparison of modeled oxygen distributions

https://doi.org/10.5194/egusphere-2025-2631
Preprint. Discussion started: 29 July 2025

with experimental measurements reveals that simulated values of the oxygenated zone was slightly lower than observed. This discrepancy is mainly attributed to two factors: firstly, the dissolved oxygen concentrations measured by the planar optode system were relatively high, as noted in Wolke et al. (2019) themselves. Secondly, only oxygen fluxes within immobile riverbeds were simulated and did not include the areas of the mobile sections in the numerical modeling. Because the mobile riverbeds exist in oxygen-rich environments, this exclusion led to the simulated values being lower than the measured values. Overall, the simulated hyporheic exchange flux, oxygen area and oxygen fluxes are displayed in Figure 3 and they are in good agreement with the measurements of Wolke et al. (2019) in trend, suggesting that the mobile bedform model is capable to reproduce realistic conditions well.

3.2 Effect of bedform migration on mixing regimes and solute transport

To simulate the range of natural environmental conditions, the reactive transport equations were solved for different stream velocities, grain sizes and groundwater upwelling fluxes, which include a corresponding range of ripple migration celerites and sediment permeabilities derived from the empirical relations. As an example, the patterns of pore water transport as well as SW and GW mixing are shown for a grain size of 0.15 mm, a constant ratio between pumping driven hyporheic exchange flux and upwelling GW flux $U_b = 0.6$ and four different stream velocities, that is four different *Re* numbers.

For low surface water flow velocity (*Re* = 2500, $U = 0.125$ m/s), no migration of bedform was predicted by the model. SW enters the sediment in the high-pressure region on the stoss side, flows through the porous medium, and exits the bedform in the low-pressure region on the lee side, forming a typical conchoidally shaped hyporheic flow cell. Upwelling GW is diverted around the

https://doi.org/10.5194/egusphere-2025-2631
Preprint. Discussion started: 29 July 2025

367 hyporheic flow cell, mixes with SW, and then exits into the overlying water from both sides, in
368 patterns similar to those shown previously by Fox et al. (2014) and Hester et al., (2019). SW and GW
369 mixing zone (i.e. the mixing area where the fraction of GW ranges between 16% and 84%) emerges
370 as a thin band along the hyporheic flow cell, and covers over 8 % of the modeled domain.
371 Meanwhile, NMD denitrification occurs below the oxygen plume with the reactive zone in a
372 conchoidal shaped distribution, while MD denitrification reactive zone develops along the edge of
373 the mixing zone, where DOC from SW meets nitrate from GW (see row 1 in Figure 4).

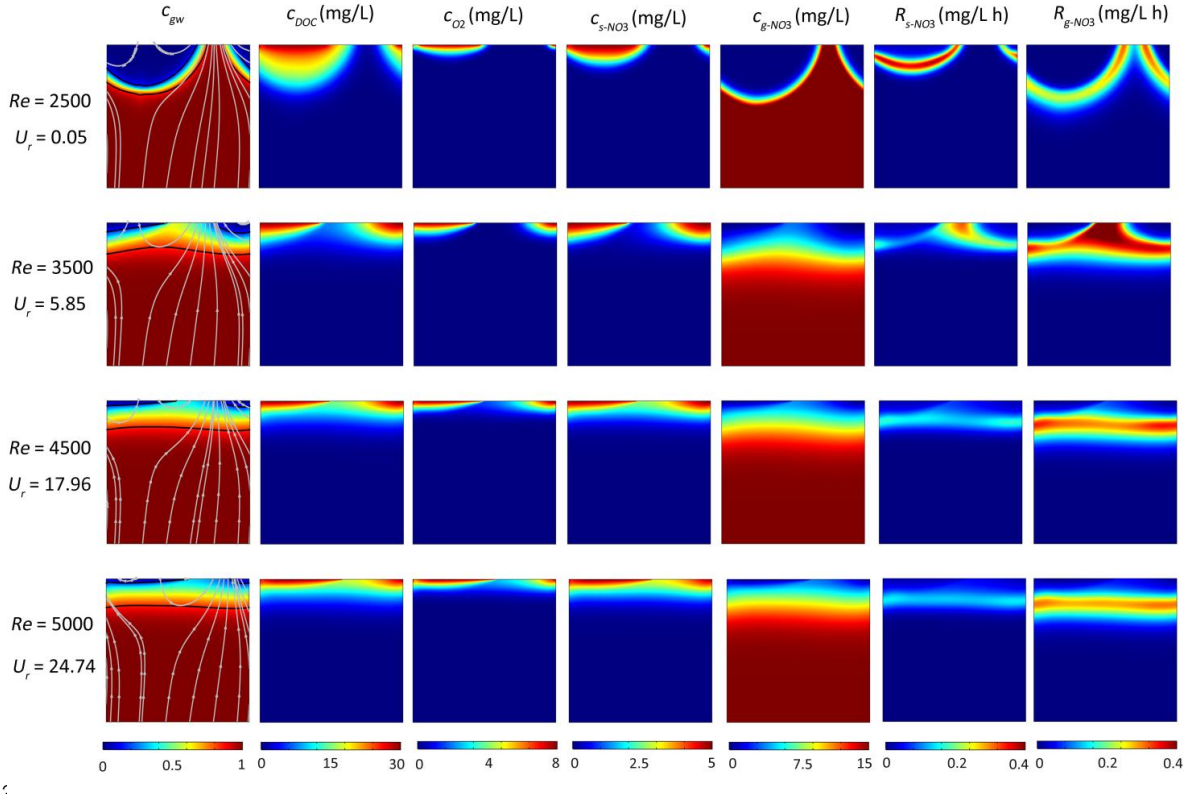

375 **Figure 4.** Effect of bedform migration on riverbed biogeochemistry for U_b = 0.6 and D_{50} = 0.15 mm.
376 Shown are profiles of (column 1) conservation solute representing groundwater fraction (c_{gw}),

https://doi.org/10.5194/egusphere-2025-2631
Preprint. Discussion started: 29 July 2025

(column 2) DOC concentration (c_{DOC}), (column 3) O_2 concentration (c_{O2}), (column 4) s-NO_3^- concentration ($c_{s\text{-}NO3-}$), (column 5) g-NO_3^- concentration ($c_{g\text{-}NO3-}$), (column 6) non-mixing-dependent (NMD) denitrification rate ($R_{s\text{-}NO3-}$) and (column 7) mixing-dependent (MD) denitrification rate ($R_{g\text{-}NO3-}$).

As stream flow velocity increases (Re = 3500, U = 0.175 m/s), this changes the pressure distribution patterns with its zones of high and low pressure. Consequently, the simulated hyporheic flow cells move downstream, while simultaneously also shrinking in size. The shape of the SW and GW mixing zone changes distinctly, forming a horizontal band with a wider range 17.01% of the while domain. The penetration of stream-derived solutes into the streambed is reduced, with a more gradual concentration gradient in the horizontal and vertical directions, whereas the g-NO_3^- plume is uniformly distributed horizontally. Both NMD and MD denitrification hot spots form in the central position near the sediment-water interface as the bedform surface (see row 2 in Figure 4).

When bedform migration is further increased (U_r = 17.96 and 24.74), the bedform migration fully dominates over the pore water flow, and hence, continuous solute layers are found in the subsurface (as depicted in row 3 and 4 of Figure 4). The penetration depths of stream-borne solutes are decreased in comparison to those in slow- to medium- fast migrating bedforms. The NMD and MD denitrification zones become thin and move upward with decreased reaction rates. Similar to the conclusions obtained in previous studies (Kessler et al., 2015; Zheng et al., 2019), the migration of the bedform reduces the penetration depth of solute and the scope of hyporheic exchange cell. We also found that a larger migration celerity increases the size of mixing zone between surface water and groundwater. The SW and GW mixing zone accounts for 17.74% and 17.86% of the domain area, respectively.

https://doi.org/10.5194/egusphere-2025-2631
Preprint. Discussion started: 29 July 2025

3.3 Effect of migration celerity on mixing regimes

The mixing intensity across the bedform surface and the size of the mixing area within the subsurface are estimated by simulating four different grain sizes and five upwelling groundwater fluxes, under varying stream velocities associated with the corresponding bedform celerity. The evolutions of the hyporheic exchange flux, net mixing flux and size of mixing zone with increasing *Re* number are summarized in Figure 5. In the third row of Figure 5, *Fmix* represents the ratio of the net mixing flux to the total hyporheic exchange flux. This total flux is triggered by both pumping and bedform migration, and is simultaneously influenced by upwelling groundwater. *Fmix* serves as a metric to quantify the proportion accounted for by the surface water-groundwater mixing flux within the overall flux of surface water and groundwater interaction across the sediment-water interface.

As shown in Figure 5, the hyporheic exchange flux increases as the stream velocity and bedform celerity rise across various grain sizes of the bedform, meanwhile the mixing flux across the sediment-water interface also increases with the increasing stream velocity, except for some special circumstances. For riverbed consists of very fine and fine sand (D_{50} = 0.08−0.15 mm) under moderate groundwater discharging conditions (U_b < 0.5), the mixing flux increases significantly at the start of bedform migration, and then the mixing flux across the sediment-water interface begins to decline with increasing celerity. In fact, this is because higher migration velocities of a riverbed with relatively low permeability limits the discharge of groundwater into the river (a horizontal distribution of stream borne solute plume), leading to the mixing of SW and GW primarily occurring within the streambed (see the column 1 in Figure 4). Concurrently, only the mixing flux through the water-sediment interface is reduced at this time.

For medium sand (D_{50} = 0.22−0.36 mm), we found that the SW and GW mixing flux

https://doi.org/10.5194/egusphere-2025-2631
Preprint. Discussion started: 29 July 2025

421 demonstrates a substantial increase relative to stationary bedforms when bedform migration initiates
422 at moderate velocities. As migration celerity accelerates, the magnitude of mixing flux gradually
423 approaches a plateau, with only marginal reductions observed at higher migration celerities. Besides,
424 the size of SW and GW mixing zone also exhibit the similar trends.

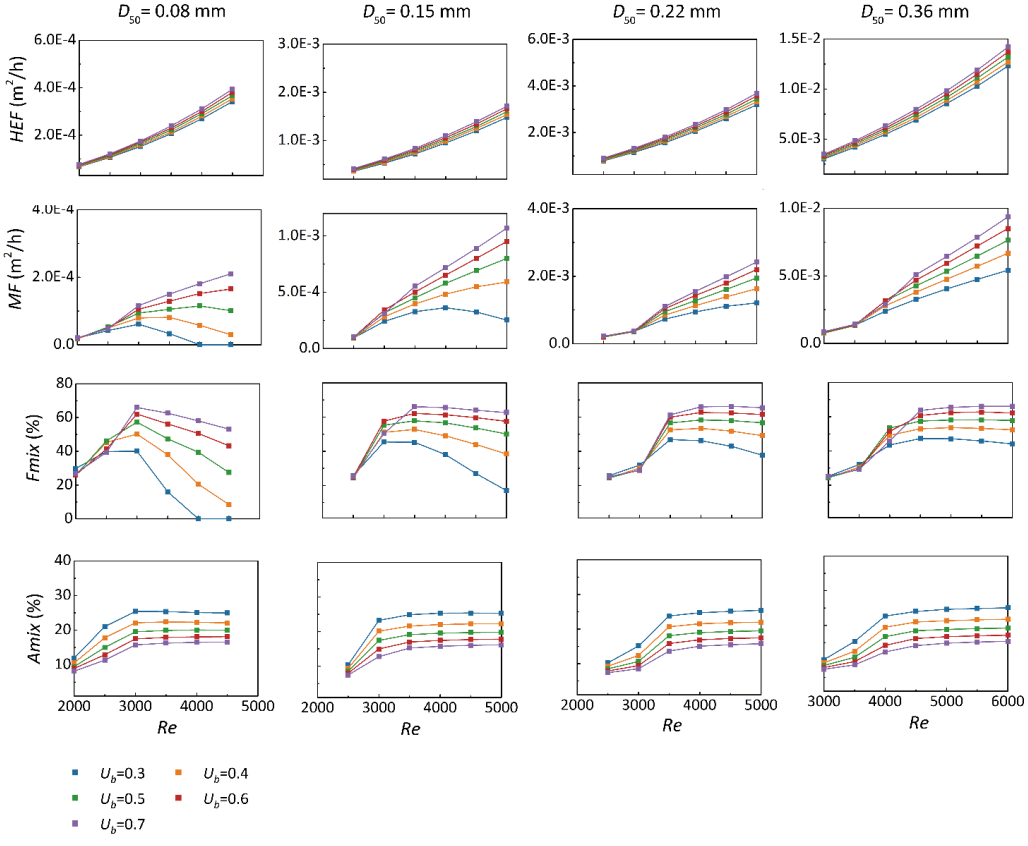

425

426 **Figure 5.** The variation of hyporheic exchange flux (*HEF*, row 1) and mixing flux (MF, row 2)
427 across the sediment-water interface, the proportion of mixing flux to hyporheic exchange flux (*Fmix*,
428 row 3) and size of mixing zone (*Amix*, row 4) with stream velocity and associated bedform celerity
429 across different medium grain size when U_b = 0.3−0.7.

https://doi.org/10.5194/egusphere-2025-2631
Preprint. Discussion started: 29 July 2025

Overall, bedform migration controls the shape and size of the SW and GW mixing zone, enhances the magnitude of hyporheic exchange flux and mixing flux. The mixing flux and size is also influenced by the upwelling GW flux. As U_b increases from 0.3 to 0.6, the mixing flux and the proportion of mixing flux to total hyporheic exchange flux rise significantly. An increase in U_b reduces the size of the mixing zone because both the hyporheic exchange flow cell and the mixing zone are confined to shallower depths within the riverbed due to the larger upward flow.

3.4 Impact of ripples migration on nitrate removal

To assess the impact of ripple migration on the removal of s-NO_3^- and g-NO_3^- within domains of varying medium grain sizes, the influx of nitrate into the riverbed and the total reaction rate were determined.

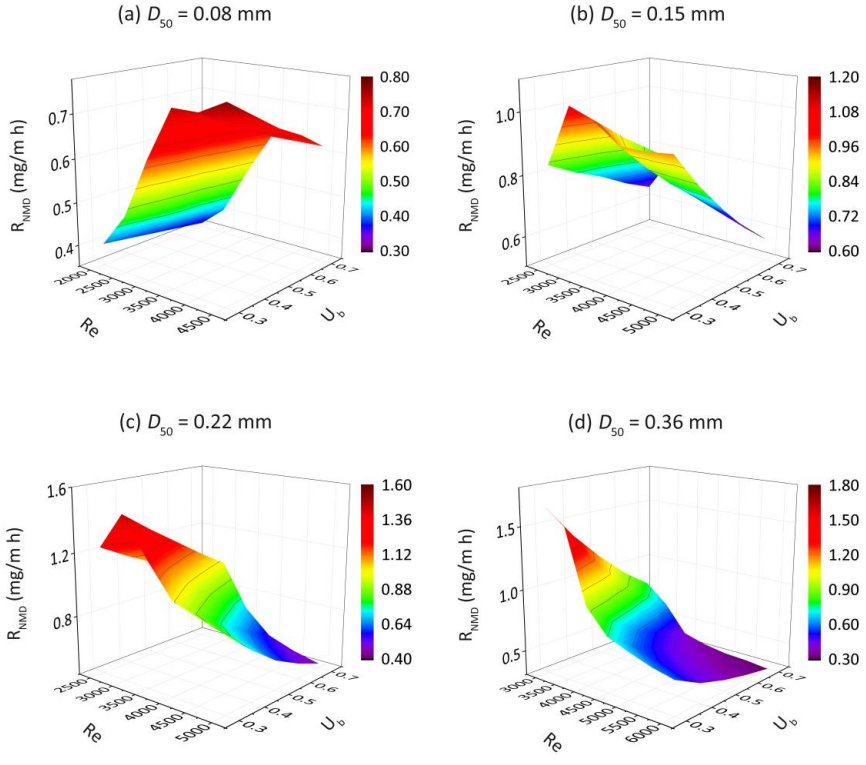

Figure 6. The non-mixing-dependent denitrification rates (R_{NMD}) as functions of U_b and *Re* for

https://doi.org/10.5194/egusphere-2025-2631
Preprint. Discussion started: 29 July 2025

different medium grain sizes.

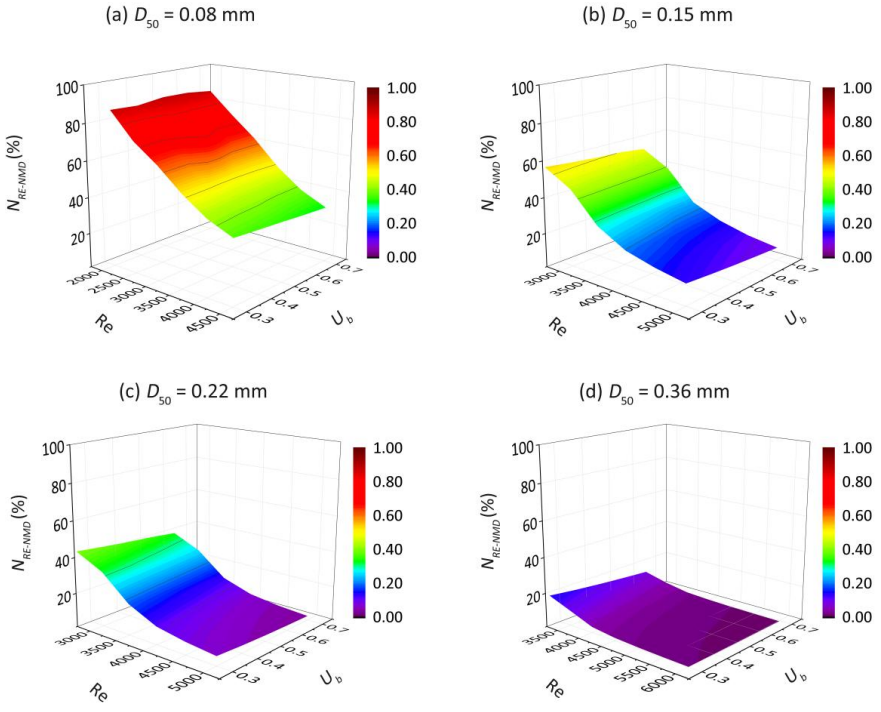

Figure 7. The removal efficiencies of stream borne nitrate (N_{RE-NMD}) as functions of U_b and Re for different medium grain sizes.

For s-NO_3^-, the NMD denitrification rate increases with both the overlying water velocity and the migration celerity in very fine sand (D_{50} = 0.08 mm). This is likely caused by higher flow velocities driving longer advective flow paths and increase solute residence times within the sediment, thereby enhancing denitrification in reaction-limited systems (Da > 2.85). In contrast, in riverbeds of fine to medium sand (D_{50} = 0.15−0.36 mm) with higher permeabilities, the reduction rate of s-NO_3^- is negatively correlated with the mean stream velocity when the system becomes transport-limited (Da < 2). This is likely because nitrate travels fast along flow paths and does not undergo denitrification within the moving bedforms (Figure 6). Additionally, the migrating bedforms

https://doi.org/10.5194/egusphere-2025-2631
Preprint. Discussion started: 29 July 2025

454 enhance the delivery of s-NO_3^- into the sediment due to increased hyporheic exchange flux.
455 Consequently, the removal efficiency of s-NO_3^- decreases monotonically across various medium
456 grain sizes (Figure 7).

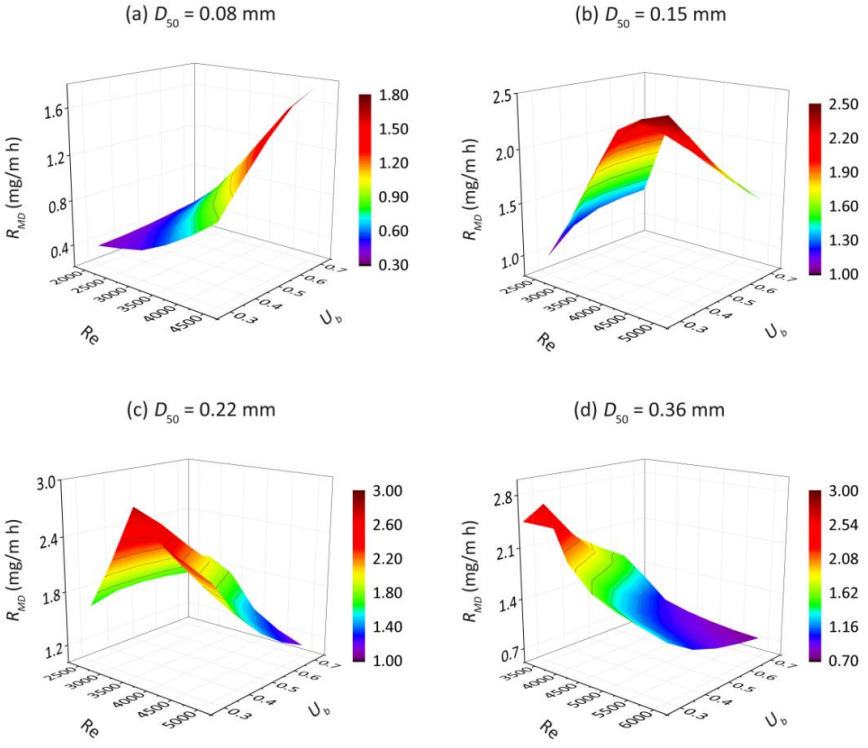

457

458 **Figure 8.** The mixing-dependent denitrification rates (R_{MD}) as functions of U_b and Re for different
459 medium grain sizes.

460 For g-NO_3^-, the increase in MD denitrification is also seen for g-NO_3^- at low to medium Re
461 when D_{50} < 0.36 mm (Figure 8). Compared to s-NO_3^-, the advective flow paths and residence times
462 of g-NO_3^- in groundwater are longer. Consequently, the reduction rate of g-NO_3^- decreases only in
463 riverbeds consisting of medium sand with fast bedform migration celerity (Re > 4000), as the solute
464 residence time is significantly reduced. Interestingly, the rise in the MD denitrification rate

https://doi.org/10.5194/egusphere-2025-2631
Preprint. Discussion started: 29 July 2025

compensates for the increased nitrate influx in very fine sand (D_{50} = 0.08 mm) at high stream velocity. Most of g-NO_3^- that enters the sediment is consumed before entering the overlying water column. For fine to medium sand riverbed (D_{50} = 0.15–0.36 mm), the g-NO_3^- removal efficiency decreases strongly with increasing *Re*. The natural protective role of the SW and GW mixing zone in preventing nitrate-contaminated groundwater from entering rivers is being hindered (Figure 9).

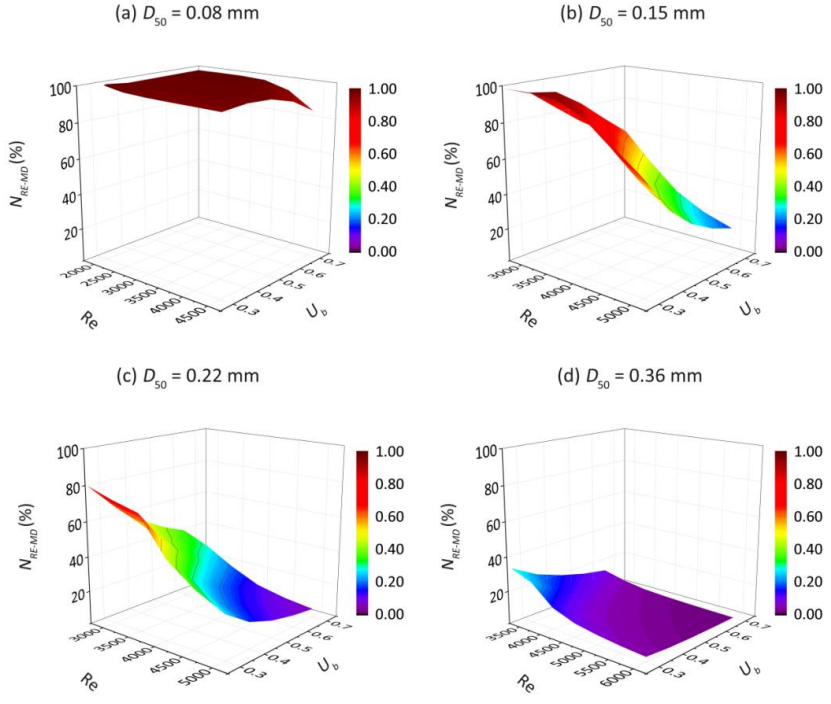

Figure 9. The removal efficiencies of groundwater borne nitrate (N_{RE-MD}) as functions of U_b and *Re* for different medium grain sizes.

4. Discussion

This study for the first time quantified the effect of bedform migration on surface water and groundwater mixing process as well as mixing triggered denitrification. Previous research has primarily focused on the potential impacts of bedform migration on hyporheic exchange driven by streambed morphological features, as well as non-mixing-dependent biogeochemical processes

https://doi.org/10.5194/egusphere-2025-2631
Preprint. Discussion started: 29 July 2025

where reactants are assumed to reside predominantly in surface water. However, such studies represent only a small subset of possible streambed environmental conditions, focusing exclusively on specific headwater stream conditions (Jiang et al., 2022; Kessler et al., 2015; Ping et al., 2022; Zheng et al., 2019). The impact of bedform migration on the conceptual model of bedform-induced hyporheic exchange, which is influenced by groundwater upwelling and/or ambient lateral groundwater flow in the mid-stream section of lowland rivers, has received relatively less attention and examination.

In streams and rivers that are fed by regional groundwater and possess undulating bedforms, surface water gets mixed with groundwater throughout the local hyporheic exchange process. The mixing zone exhibits a typical crescent shape along the periphery of typical hyporheic exchange cells within a stationary streambed (as reported by Fox et al., 2014; Hester et al., 2019; Nogueira et al., 2022). The sizes of the surface water-groundwater mixing zone (e.g., thickness and area) occupy a small proportion of the whole HZ. In the immobile bedform, the thin mixing zones (16 ~ 84% ranges) occupying ~10% is consistent with prior work (Hester et al., 2013; Santizo et al., 2020). During the initiation of bedform migration, however, the mixing pattern, size, and intensity of surface water-groundwater interactions undergo modification. A continuous SW-GW mixing zone is formed within the ripples of the medium- to fast-moving bedform (Figure 4), and the area of mixing zone increases to approximately 15 ~ 25% at this time. Besides, the net flux of surface water and groundwater mixing across the sediment-water interface (or within the riverbed) is also increased with stream velocity and bedform migration celerity (Figure 5). As a result, bedform migration controls and determines the hotspots and magnitude of the SW and GW mixing. The bedforms are typically assumed to be immobile potentially making underestimations of surface water and

https://doi.org/10.5194/egusphere-2025-2631
Preprint. Discussion started: 29 July 2025

groundwater mixing flux and mixing zone in a HZ.

Instead of the typical crescent-shaped mixing-dependent (MD) denitrifying zone observed in stationary bedforms (Naranjo et al., 2015; Hester et al., 2014, 2019), the MD reaction zonation changes to the layer shape distributed at the fringe of the HEF cells, where mixing between SW and GW develop to a largest degree (Figure 5). Such a situation exists where the stream flows into with a relative homogeneous sandy riverbed with low autochthonous organic carbon content and encounters with nitrate enrich groundwater. The heterogeneous streambeds including buried autochthonous organic matter (Sawyer, 2015; Ping et al., 2022), deposited particulate organic particles (Drummond et al., 2017; Ping et al., 2023), and biological aggregate (Xian et al., 2022), would complicate the hyporheic exchange process, induce the rough and irregular shapes and boundaries of HEF cells and mixing zone, and therefore affect redox microenvironments and biogeochemical zonations. MD denitrifying hotspot would also occur around available sources of DOC.

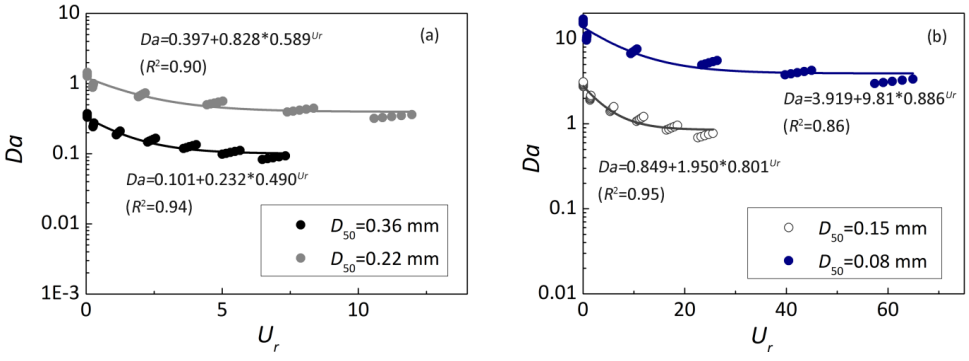

Figure 10. Variation of the dimensionless Damköhler number as a function of the dimensionless parameter U_r.

Previous studies have demonstrated that migrating bedforms constrains the penetration depths of stream-borne solute and reduces the removal efficiency of stream-borne nitrate (Jiang et al., 2022;

https://doi.org/10.5194/egusphere-2025-2631
Preprint. Discussion started: 29 July 2025

Kessler et al., 2015; Ping et al., 2022; Zheng et al., 2019). Our results revealed that the bedform migration also reduces the HZ attenuation ability for groundwater borne nitrate. However, the reasons for this phenomenon are different for various riverbed sediments. For very fine sand (D_{50} = 0.08 mm), a larger celerity results in a decline in transport timescale with less impact on removal efficiency as the system is rate-limited ($Da >> 1$). For fine to medium sand riverbed (D_{50} = 0.15–0.36 mm), the transport-limited situation leads to a low denitrification rate with increasing U_r but constantly decreasing Da ($Da < 1$). It is important to note that the reaction timescale we calculated is based on the consumption period of oxygen to a prescribed anoxic threshold. Under these conditions, the exhaustion of labile DOC would also lead to the cessation of denitrification (Zarnetske et al., 2011a, 2011b). These results demonstrate that in order to evaluate the self-purification capacity of the HZ and its function as a natural barrier mitigating groundwater contamination, riverbed sediment transport dynamics and grain size distributions need to be considered. Stabilizing bedform configurations in restoration projects would enhances the natural attenuation capacity of the HZ.

Different from previous studies that demonstrated the magnitude of NMD denitrification was often greater than that of MD denitrification (Hester et al., 2014; Trauth and Fleckenstein, 2017). The results in our study show that the total reaction rate of s-NO_3^- was smaller than that of g-NO_3^- in mobile bedforms. This phenomenon can be attributed to the following two reasons: First, the concentration of s-NO_3^- is one-third that of g-NO_3^-; Second, the reaction zone is reduced by migration celerity for NMD denitrification, while the reaction zone for MD denitrification is increased in the riverbed at the onset of bedform migration. The mixing intensity increases with bedform migration, which facilitates the MD denitrification more effectively (Hester et al., 2019; Nogueira et al., 2024; Trauth and Fleckenstein., 2017). Moreover, migration celerity increases the

https://doi.org/10.5194/egusphere-2025-2631
Preprint. Discussion started: 29 July 2025

influx of nitrate into the HZ by enhanced hyporheic exchange, while it has less impact on upwelling GW flux. Hence, the removal efficiency of g-NO_3^- is also higher than that of s-NO_3^- in these scenarios. More attention should be paid to the mixing dynamics and mixing triggered biogeochemical reactions, which is helpful to put forward appropriate stream restoration plans so as to enhance the health of the aquatic ecosystem (Hester et al., 2017; Lawrence et al., 2013).

In this study, we focused on ripples and, more broadly, shorter-wavelength topographic roughness elements that form under low subcritical flow conditions in sandy riverbeds (Ashley, 1990; Gomez-Velez et al., 2015; Raudkivi, 1997). The undulating bedforms maintain dynamic equilibrium through geometric adjustments, with their geometry remaining unchanged as the stream velocity fluctuates within a specific range (10–30 cm/s). When stream velocities exceed this upper threshold, a condition commonly observed in fast-flowing rivers, bedform geometries can be altered, ultimately leading to bedform erosion (Boano et al., 2013; Harvey et al., 2012). This process is not accounted for in the current model. If small-scale ripples develop and merge with larger-scale ripples and dunes under moderate stream velocities, the removal efficiency of s-NO_3^- and g-NO_3^- may be enhanced due to the extended hyporheic flow paths and increased residence timescales (Harvey et al., 2012; Zomer and Hoitink, 2024). Otherwise, the removal of s-NO_3^- would be highly hindered because of shorter residence time and fully oxic condition in fast moving bedforms and fast flowing rivers, while the removal of g-NO_3^- would likely be less affected within the immobile streambeds.

In our model, dissimilatory nitrate reduction to ammonium (DNRA) was not incorporated, given that denitrification is typically regarded as the predominant pathway for nitrate removal, whereas DNRA plays a secondary role in nitrate transformation (Zarnetske et al., 2012). Lansdown et al. (2012) and Quick et al. (2016) have demonstrated that approximately 5% of $^{15}NO_3^-$ tracer in river

https://doi.org/10.5194/egusphere-2025-2631
Preprint. Discussion started: 29 July 2025

sediment incubations underwent DNRA, while 85% underwent denitrification. Nevertheless, DNRA competes with denitrification for NO_3^- and DOC as electron acceptor and donors within HZs. When an oligotrophic and/or a pristine stream infiltrate into the streambed and subsequently interact and mix with nitrate-enriched groundwater, the MD DNRA would not occur due to the low C/N ratio. MD denitrification zone shifts upstream toward the overlying water column, leading to a pronounced spatial mismatch between the denitrification zone and the mixing interface. This occurs because DOC is intensively consumed within the HEF cell, such that elevated MD denitrification rates emerge below the DOC and oxygen plumes yet above the mixing zone. Specifically, this phenomenon can be attributed to the critical role of dispersion effect in solute transport and mixing-triggered denitrification, besides advection effect. When an eutrophication stream with higher DOC concentration, DNRA would have a greater influence in nitrate transformation because DNRA is prone to occur in NO_3^--limited (that is DOC sufficient) conditions compared to denitrification (Zhu et al., 2023). The ammonia produced by mixing-dependent DNRA would be further nitrified within the aerobic HEF cell, thereby potentially elevating the risk of nitrate pollution in surface water.

In our model, stream velocity and upward groundwater flux are considered constant in the present model, yet they may change in time due to storm events, tidal pumping, snowmelt, or reservoir hydro-peaking (Liu et al., 2024; Nogueira et al., 2022; Song et al., 2018). Hester et al. (2019) demonstrated that increasing surface water stage would enhance both NMD and MD denitrification. Nogueira et al. (2024) and Trauth and Fleckenstein (2017) pointed out that groundwater discharge events increase the magnitude of surface water-groundwater mixing, therefore effecting the prevalence of MD denitrification. The interactions among morphological dynamics, hyporheic exchange, and biogeochemical processes under transient conditions are key

https://doi.org/10.5194/egusphere-2025-2631
Preprint. Discussion started: 29 July 2025

areas for future research.

5. Conclusion

The numerical model developed in this study was applied to simulate the interaction and mixing of upwelling groundwater with bedform-induced hyporheic flow, examining how bedform migration influences surface water and groundwater mixing and the processing of groundwater-borne nitrate within the HZ. Our analysis quantified the mixing flux and the size of mixing zone, as well as the mixing-dependent denitrification rates and removal efficiencies across riverbed sediments characterized by varying grain sizes, stream flow velocities, and groundwater discharge fluxes. These model simulations reveal that as bedforms migrate, the surface water-groundwater mixing zone and the associated mixing-dependent denitrification zone progressively evolve into uniform, band-like structures. For riverbeds composed of fine to medium sand (D_{50} = 0.15–0.36 mm), both the magnitudes of SW and GW exchange flux and mixing flux increase significantly when turnover becomes the dominant exchange mechanism, while the proportion of mixing flux across the sediment-water interface and the size of mixing zone remain approximately constant at this time. Meanwhile, both the mixing-dependent denitrification rates and removal efficiencies decline significantly with increasing stream flow velocities and associated bedform migration rates. Under dynamic bedform conditions, the self-purification capacity of the HZ is reduced, compromising its role as a natural barrier against groundwater contamination. The management of aquatic systems involving riverbed sediments can be enhanced by incorporating the analyzed factors identified here, particularly when management goals encompass the removal of groundwater borne nitrate.

https://doi.org/10.5194/egusphere-2025-2631
Preprint. Discussion started: 29 July 2025

603 **Notation**

S	Stream slope [-]
H	Water depth [L]
U	Stream velocity [L T^{-1}]
λ	Ripple wavelength [L]
u_c	Bedform migration celerity [L T^{-1}]
l	Streambed height [L]
H_d	Ripple height [L]
D_{50}	Median sediment size [L]
x	Horizontal coordinate, rightward positive [-]
y	Vertical coordinate, upward positive [-]
k	Sediment permeability [L^2]
K	Sediment hydraulic conductivity [L T^{-1}]
h	Hydraulic head [L]
h_m	Amplitude of the sinusoidal head variation [L]
m	Wavenumber of the variation [-]
g	Gravity acceleration [L T^{-2}]
c_i	Concentration of reactive components [M L^{-3}]
c_{gw}	Groundwater tracer [M L^{-3}]
v	Seepage velocity [L T^{-1}]
θ	Sediment porosity [-]
α_L	Longitudinal dispersivities

https://doi.org/10.5194/egusphere-2025-2631
Preprint. Discussion started: 29 July 2025

α_T	Transverse dispersivities [L]
$\boldsymbol{D_{ij}}$	Hydrodynamic dispersion [L^2 T^{-1}]
D_m	Molecular diffusion coefficient [L^2 T^{-1}]
ι	Tortuosity factor [-]
V_{AR}	Maximum reaction rate of aerobic respiration [T^{-1}]
V_{DN}	Maximum reaction rate of denitrification [T^{-1}]
K_{inh}	Non-competitive inhibition factor [M L^{-3}]
K_{DOC}	Half-saturation for dissolved organic carbon [M L^{-3}]
K_{NO3}^-	Half-saturation for nitrate [M L^{-3}]
K_{O2}	Half-saturation for oxygen [M L^{-3}]
X_{AR}	Microbial concentration facilitating aerobic respiration [M L^{-3}]
X_{DN}	Microbial concentration facilitating denitrification [M L^{-3}]
ρ_s	Sediment density [M L^{-3}]
ρ	Water density [M L^{-3}]
P	Hydraulic pressure [M $L^{-1}T^{-2}$]
u^*	Bed shear velocity [L T^{-1}]
u_{cr}^*	Critical bed shear velocity [L T^{-1}]
n	Manning coefficient [-]
τ^*	Shield parameter [-]
τ_{cr}	Critical shear stress [M $L^{-1}T^{-2}$]
τ_{cr}^*	Critical Shield parameter [-]
r	Submerged specific gravity of sediment [-]

https://doi.org/10.5194/egusphere-2025-2631
Preprint. Discussion started: 29 July 2025

R_{O2}	Aerobic respiration rate [M $L^{-3}T^{-1}$]
$R_{s\text{-}NO3}$	Non-mixing-dependent denitrification rate [M $L^{-3}T^{-1}$]
$R_{g\text{-}NO3}$	Mixing-dependent denitrification rate [M $L^{-3}T^{-1}$]
R_{DOC}	Dissolved oxygen carbon consumption rate [M $L^{-3}T^{-1}$]
υ	Kinematic viscosity of water [L^2 T^{-1}]
u_s	Underflow seepage velocity induced by stream gradient [L T^{-1}]
Re	Reynolds number [-]
U_r	ratio of bedform celerity to pore water velocity [-]
u_p	Darcy velocity induced by pumping process [L T^{-1}]
u_q	Vertical groundwater flux [L T^{-1}]
U_b	Ratio of vertical groundwater flux to hyporheic exchange flux
τ_R	Biogeochemical reaction timescale [T]
τ_T	Water transport timescale [T]
Da	Damköhler number [-]
Δx	Bedform migrating displacement per timestep (L)
dt	The length of per timestep (T)
Da'	Conversion factor for unit Darcy to m^2 [-]
F_{mix}	the proportion of mixing flux to hyporheic exchange flux [-]
A_{mix}	Surface water and groundwater mixing zone [L^2]
A	Streambed area [L^2]
M_{NDN}	Nitrate removed by non-mixing dependent denitrification [M]
M_{DN}	Nitrate removed by mixing dependent denitrification [M]

https://doi.org/10.5194/egusphere-2025-2631
Preprint. Discussion started: 29 July 2025

N_{RE}	Nitrate removal efficiency [-]
M_{in}	Nitrate being introduced into streambed [M]

Abbreviations

HZ	Hyporheic zone
SW	Surface water
GW	Groundwater
HEF	Hyporheic exchange flow
MF	Mixing flux
NMD	Non-mixing dependent
MD	Mixing dependent
AR	Aerobic respiration
DN	Denitrification

Supporting information

Additional details of the model scenarios and model validation were displayed in the supporting information.

Data availability

All raw data can be provided by the first author upon request.

Competing interest

The authors declare that they have no conflict of interest.

Author contribution

https://doi.org/10.5194/egusphere-2025-2631
Preprint. Discussion started: 29 July 2025

Conceptualization: XP, YX

Formal analysis: XP

Funding acquisition: XP, ZW, YX, SK

Investigation: XP, ZW

Methodology: XP, ZW, YX

Writing-original draft: XP

Writing-review and editing: ZW, YX, MJ, SK

Project administration: ZW

Acknowledgments

The work was financially supported by the National Natural Science Foundation of China (Nos. U23A2042, 42407075 and 42107089). This study was also supported by the "CUG Scholar" Scientific Research Funds at China University of Geosciences (Wuhan) (Project No.2023067), and supported by the Postdoctoral Fellowship Program of China Postdoctoral Science Foundation under Grant Number GZC20241601. SK has been supported by the Royal Society (INF\R2\212060).

Reference

Ahmerkamp, S., Winter, C., Janssen, F., Kuypers, M. M., and Holtappels, M.: The impact of bedform migration on benthic oxygen fluxes, J. Geophys. Res.: Biogeosci. 120, 2229–2242, https://doi.org/10.1002/2015JG003106, 2015.

https://doi.org/10.5194/egusphere-2025-2631
Preprint. Discussion started: 29 July 2025

630 Ahmerkamp, S., Winter, C., Krämer, K., Beer, D. D., Janssen, F., Friedrich, J., Kuypers, M. M. M.,
631 and Holtappels, M.: Regulation of benthic oxygen fluxes in permeable sediments of the coastal
632 ocean, Limnol. Oceanogr. 62(5), 1935–1954, http://doi.org/10.1002/lno.10544, 2017.

633 Ascott, M. J., Stuart, M. E., Gooddy, D. C., Marchant, B. P., Talbot, J. C., Surridge, B. J., and Polya,
634 D. A.: Provenance of drinking water revealed through compliance sampling, Environ. Sci.:
635 Processes & Impacts, 21(6), 1052-1064, https://doi.org/10.1039/C8EM00437D, 2019.

636 Ashley, G. M.: Classification of large-scale subaqueous bedforms: A new look at an old problem-
637 SEPM bedforms and bedding structures, J. Sediment. Res. 60(1), 160–172,
638 https://doi.org/10.1306/212F9138-2B24-11D7-8648000102C1865D, 1990.

639 Azizian, M., Grant, S. B., Kessler, A. J., Cook, P. L. M., Rippy, M. A., and Stewardson, M. J.:
640 Bedforms as biocatalytic filters: a pumping and streamline segregation model for nitrate
641 removal in permeable sediments, Environ. Sci. Technol. 49, 10993–11002,
642 https://doi.org/10.1021/acs.est.5b01941, 2015.

643 Bartholdy, J., Ernstsen, V. B., Flemming, B. W., Winter, C., Bartholomä, A., and Kroon, A.: On the
644 formation of current ripples, Sci. Rep. 5(1), 11390, https://doi.org/10.1038/srep11390, 2015.

645 Bear, J., and Verruijt, A.: Modeling groundwater flow and pollution. D. Reidel Publishing Company,
646 1998.

647 Boano, F., Harvey, J. W., Marion, A., Packman, A. I., Revelli, R., Ridolfi, L., and Wörman, A.:
648 Hyporheic flow and transport processes: Mechanisms, models, and biogeochemical
649 implications, Rev. Geophys. 52, 603–679, https://doi.org/10.1002/2012RG000417, 2014.

https://doi.org/10.5194/egusphere-2025-2631
Preprint. Discussion started: 29 July 2025

650 Boano, F., Poggi, D., Revelli, R., and Ridolfi, L.: Gravity-driven water exchange between streams
651 and hyporheic zones, Geophys. Res. Lett. 36, L20402, https://doi.org/10.1029/2009GL040147,
652 2009.

653 Boano, F., Revelli, R., and Ridolfi, L.: Water and solute exchange through flat streambeds induced by
654 large turbulent eddies, J. Hydrol. 402, 290–296, https://doi.org/10.1016/j.jhydrol.2011.03.023,
655 2011.

656 Boano, F., Revelli, R., and Ridolfi, L.: Modeling hyporheic exchange with unsteady stream discharge
657 and bedform dynamics, Water Resour. Res. 49(7), 4089–4099,
658 https://doi.org/10.1002/wrcr.20322, 2013.

659 Boulton, A. J., Findlay, S., Marmonier, P., Stanley, E. H., and Valett, H. M.: The functional
660 significance of the hyporheic zone in streams and rivers, Annu. Rev. Ecol. Syst. 29(1), 59–81,
661 https://doi.org/10.1146/annurev.ecolsys.29.1.59, 1998.

662 Briggs, M. A., Lautz, L. K., Hare, D. K., and González-Pinzón, R.: Relating hyporheic fluxes,
663 residence times, and redox-sensitive biogeochemical processes upstream of beaver dams,
664 Freshw. Sci. 32, 622–641, https://doi.org/10.1899/12-110.1, 2013.

665 Burt, T. P., Howden, N. J. K., Worrall, F., Whelan, M. J., and Bieroza, M.: Nitrate in United Kingdom
666 rivers: Policy and its outcomes since 1970, Environ. Sci. Technol., 45(1), 175–181,
667 https://doi.org/10.1021/es101395s, 2011.

668 Cardenas, M. B.: Hyporheic zone hydrologic science: A historical account of its emergence and a
669 prospectus. Water Resour. Res. 51, 3601–3616, https://doi.org/10.1002/2015WR017028, 2015.

https://doi.org/10.5194/egusphere-2025-2631
Preprint. Discussion started: 29 July 2025

Cardenas, M. B., and Wilson, J. L.: The influence of ambient groundwater discharge on exchange zones induced by current-bedform interactions, J. Hydrol. 331, 103–109, https://doi.org/10.1016/j.jhydrol.2006.05.012, 2006.

Cardenas, M. B., Wilson, J. L., and Haggerty, R.: Residence time of bedform-driven hyporheic exchange, Adv. Water Resour. 31(10), 1382–1386, https://doi.org/10.1016/j.advwatres.2008.07.006, 2008.

Coleman, S. E., and Melville, B. W.: Bed-form development, J. Hydraul. Eng. 120(5), 544–560, https://doi.org/10.1061/(ASCE)0733-9429(1994)120:5(544), 1994.

Conley, D. J., Paerl, H. W., Howarth, R. W., Boesch, D. F., Seitzinger, S. P., Havens, K. E., Lancelot, C., and Likens, G. E.: Ecology: controlling eutrophication: nitrogen and phosphorus, Science 323, 1014–1015, https://doi.org/10.1126/science.1167755, 2009.

Drummond, J. D., Larsen, L. G., González-Pinzón, R., Packman, A. I., and Harvey, J. W.: Fine particle retention within stream storage areas at base flow and in response to a storm event: Particle retention stream storage areas, Water Resour. Res. 53, 5690–5705, https://doi.org/10.1002/2016WR020202, 2017.

Elliott, A. H., and Brooks, N. H.: Transfer of nonsorbing solutes to a streambed with bed forms: Theory, Water Resour. Res. 33(1), 123–136, https://doi.org/10.1029/96wr02784, 1997.

Fox, A., Boano, F., and Arnon, S.: Impact of losing and gaining streamflow conditions on hyporheic exchange fluxes induced by dune-shaped bed forms, Water Resour. Res. 50(3), 1895–1907, https://doi.org/10.1002/2013WR014668, 2014.

https://doi.org/10.5194/egusphere-2025-2631
Preprint. Discussion started: 29 July 2025

690 Gangi, A. F.: Permeability of unconsolidated sands and porous rocks. J. Geophys. Res. 90(B4),
691 3099–3104, https://doi.org/10.1029/JB090iB04p03099, 1985.

692 Gomez-Velez, J. D., Harvey, J., Cardenas, M. B., and Kiel, B.: Denitrification in the Mississippi
693 River network controlled by flow through river bedforms, Nat. Geosci. 8, 941–975,
694 https://doi.org/10.1038/NGEO2567, 2015.

695 Gu, C., Hornberger, G. M., Herman, J. S., and Mills, A. L.: Effect of freshets on the flux of
696 groundwater nitrate through streambed sediments, Water Resour. Res. 44, W05415,
697 https://doi.org/10.1029/2007WR006488, 2008.

698 Harvey, J. W., Drummond, J. D., Martin, R. L., Mcphillips, L. E., Packman, A. I., Jerolmack, D. J.,
699 Stonedahl, S. H., Aubeneau, A. F., Sawyer, A. H., and Larsen, L. G.: Hydrogeomorphology of
700 the hyporheic zone: Stream solute and fine particle interactions with a dynamic streambed, J.
701 Geophys. Res. 117(G4), G00N11, https://doi.org/10.1029/2012JG002043, 2012.

702 Hester, E. T., Cardenas, M. B., Haggerty, R., and Sourabh, S. V. A.: The importance and challenge of
703 hyporheic mixing, Water Resour. Res. 53, 3565–3575, https://doi.org/10.1002/2016WR020005,
704 2017.

705 Hester, E. T., Eastes, L. A., and Widdowson, M. A.: Effect of surface water stage fluctuation on
706 mixing-dependent hyporheic denitrification in riverbed dunes, Water Resour. Res. 55, 4668–
707 4687, https://doi.org/10.1029/2018WR024198, 2019.

708 Hester, E. T., Young, K. I., and Widdowson, M. A.: Mixing of surface and groundwater induced by
709 riverbed dunes: Implications for hyporheic zone definitions and pollutant reactions, Water
710 Resour. Res. 49, 5221–5237, https://doi.org/10.1002/wrcr.20399, 2013.

https://doi.org/10.5194/egusphere-2025-2631
Preprint. Discussion started: 29 July 2025

Hester, E. T., Young, K. I., and Widdowson, M. A.: Controls on mixing-dependent denitrification in hyporheic zones induced by riverbed dunes: A steady state modeling study, Water Resour. Res. 50, 9048–9066, https://doi.org/10.1002/2014WR015424, 2014.

Howden, N. J. K., and Burt, T. P.: Temporal and spatial analysis of nitrate concentrations from the Frome and Piddle catchments in Dorset (UK) for water years 1978 to 2007: Evidence for nitrate breakthrough? Sci. Total Environ. 407(1), 507–526, http://doi.org/10.1016/ j. scitotenv.2008.08.042, 2008.

Janssen, F., Cardenas, M. B., Sawyer, A. H., Dammrich, T., Krietsch, J., and de Beer, D.: A comparative experimental and multiphysics computational fluid dynamics study of coupled surface-subsurface flow in bed forms, Water Resour. Res. 48(8), W08514, https://doi.org/10.1029/2012WR011982, 2012.

Jiang, Q., Liu, D., Jin, G., Tang, H., Wei, Q., and Xu, J.: N2O dynamics in the hyporheic zone due to ripple migration, J. Hydrol. 610, 127891, https://doi.org/10.1016/j.jhydrol.2022.127891, 2022.

Kessler, A. J., Cardenas, M. B., and Cook, P. L. M.: The negligible effect of bed form migration on denitrification in hyporheic zones of permeable sediments, J. Geophys. Res.: Biogeosci. 120, 538–548, https://doi.org/10.1002/2014JG002852, 2015.

Krause, S., Abbott, B. W., Baranov, V., Bernal, S., Blaen, P., Datry, T., Drummond, J., Fleckenstein, J. H., Velez, J. G., Hannah, D. M., Knapp, J. L. A., Kurz, M., Lewandowski, J., Martí, E., Mendoza-Lera, C., Milner, A., Packman, A., Pinay, G., Ward, A. S., and Zarnetzke, J. P.: Organizational principles of hyporheic exchange flow and biogeochemical cycling in river

https://doi.org/10.5194/egusphere-2025-2631
Preprint. Discussion started: 29 July 2025

networks across scales, Water Resour. Res. 58 (3), e2021WR029771, https://doi.org/10.1029/2021WR029771, 2022.

Krause, S., Heathwaite, L., Binley, A., and Keenan, P.: Nitrate concentration changes at the groundwater-surface water interface of a small Cumbrian River, Hydrol. Processes, 23, 2195–2211, https://doi.org/10.1002/hyp.7213, 2009.

Krause, S., Tecklenburg, C., Munz, M., and Naden, E.: Streambed nitrogen cycling beyond the hyporheic zone: Flow controls on horizontal patterns and depth distribution of nitrate and dissolved oxygen in the upwelling groundwater of a lowland river, J. Geophys. Res.: Biogeosciences, 118, 54–67, https://doi.org/10.1029/2012JG002122, 2013.

Lansdown, K., Heppell, C. M., Dossena, M., Ullah, S., Heathwaite, A. L., Binley, A., Zhang, H., Trimmer, M., 2014. Fine-Scale in situ measurement of riverbed nitrate production and consumption in an armored permeable riverbed, Environ. Sci. Technol. 48 (8), 4425–4434, https://doi.org/10.1021/es4056005, 2014.

Lansdown, K., Heppell, C. M., Trimmer, M., Binley, A., Heathwaite, A. L., Byrne, P., and Zhang, H.: The interplay between transport and reaction rates as controls on nitrate attenuation in permeable, streambed sediments, J. Geophys. Res. Biogeosci. 120, 1093–1109, http://doi.org/10.1002/2014JG002874, 2015.

Lansdown, K., Trimmer, M., Heppell, C. M., Sgouridis, F., Ullah, S., Heathwaite, L., Binley, A., and Zhang, H.: Characterization of the key pathways of dissimilatory nitrate reduction and their response to complex organic substrates in hyporheic sediments, Limnol. Oceanogr. 57 (2), 387–400, https://doi.org/10.4319/lo.2012.57.2.0387, 2012.

https://doi.org/10.5194/egusphere-2025-2631
Preprint. Discussion started: 29 July 2025

Lawrence, J. E., Skold, M. E., Hussain, F. A., Silverman, D. R., Resh, V. H., Sedlak, D. L., Luthy, R. G., and McCray, J. E.: Hyporheic zone in urban streams: A review and opportunities for enhancing water quality and improving aquatic habitat by active management, Environ. Eng. Sci. 30, 480–501, https://doi.org/10.1089/ees.2012.0235, 2013.

Liu, F., Ding, Y., Liu, J., Latif, J., Qin, J., Tian, S., Sun, S., Guan, B., Zhu, K., and Jia, H.: The effect of redox fluctuation on carbon mineralization in riparian soil: An analysis of the hotspot zone of reactive oxygen species production, Water Res. 265, 122294, https://doi.org/10.1016/j.watres.2024.122294, 2024.

Marzadri, A., Tonina, D., and Bellin, A.: Morphodynamic controls on redox conditions and on nitrogen dynamics within the hyporheic zone: application to gravel bed rivers with alternate-bar morphology, J. Geophys. Res.: Biogeosci. 117, 184–189, https://doi.org/10.1029/2012JG001966, 2012.

Munz, M., Krause, S., Tecklenburg, C., and Binley, A.: Reducing monitoring gaps at the aquifer-river interface by modelling groundwater-surface water exchange flow patterns, Hydrol. Processes, 25, 3547–3562, https://doi.org/10.1002/hyp.8080, 2011.

Naranjo, R. C., Niswonger, R. G., and Davis, C. J.: Mixing effects on nitrogen and oxygen concentrations and the relationship to mean residence time in a hyporheic zone of a riffle-pool sequence, Water Resour. Res. 51(9), 7202–7217, https://doi.org/10.1002/2014WR016593, 2015.

Nogueira, G. E. H., Partington, D., Heidbuchel, I., and Fleckenstein, J. H.: Combined effects of geological heterogeneity and discharge events on groundwater and surface water mixing, J. Hydrol. 638, 131467, https://doi.org/10.1016/j.jhydrol.2024.131467, 2024.

https://doi.org/10.5194/egusphere-2025-2631
Preprint. Discussion started: 29 July 2025

Nogueira, G. E. H., Schmidt, C., Brunner, P., Graeber, D., and Fleckenstein, J. H.: Transit-time and temperature control the spatial patterns of aerobic respiration and denitrification in the riparian zone, Water Resour. Res. 57 (12), e2021WR030117, https://doi.org/10.1029/2021WR030117, 2021.

Nogueira, G. E. H., Schmidt, C., Partington, D., Brunner, P., and Fleckenstein, J. H.: Spatiotemporal variations in water sources and mixing spots in a riparian zone, Hydrol. Earth Syst. Sci, 26 (7), 1883–1905, https://doi.org/10.5194/hess-26-1883-2022, 2022.

Ocampo, C. J., Oldham, C. E., and Sivapalan, M.: Nitrate attenuation in agricultural catchments: shifting balances between transport and reaction, Water Resour. Res. 42(1), 85–88, https://doi.org/10.1029/2004WR003773, 2006.

Peleg, E., Teitelbaum, Y., and Arnon, S.: Exploring the influence of sediment motion on microplastic deposition in streambeds, Water Res. 249, 120952, https://doi.org/10.1016/j.watres.2023.120952, 2024.

Ping, X., Xian, Y., and Jin, M.: Influence of bedform migration on nitrate reduction in hyporheic zones of heterogeneous sediments, Water Resour. Res. 58, e2022WR033258, https://doi.org/10.1029/2022WR033258, 2022.

Ping, X., Xian, Y., and Jin, M.: Effect of particulate organic carbon deposition on nitrate reduction in the hyporheic zone, Water Resour. Res. 59, e2022WR034253, https://doi.org/10.1029/2022WR034253, 2023.

https://doi.org/10.5194/egusphere-2025-2631
Preprint. Discussion started: 29 July 2025

792 Precht, E., Franke, U., Polerecky, L., and Huttel, M.: Oxygen dynamics in permeable sediments with
793 wave-driven pore water exchange, Limnol. Oceanogr. 49(3), 693–705,
794 https://doi.org/10.2307/3597786, 2004.

795 Quick, A. M., Reeder, W. J., Farrell, T. B., Tonina, D., Feris, K. P., and Benner, S. G.: Controls on
796 nitrous oxide emissions from the hyporheic zones of streams, Environ. Sci. Technol. 50 (21),
797 11491-11500, https://doi.org/10.1021/acs.est.6b02680, 2016.

798 Raudkivi, A. J.: Ripples on stream bed, J. Hydraul. Eng. 123(1), 58–64,
799 https://doi.org/10.1061/(ASCE)0733-9429(1997)123:1(58), 1997.

800 Risse-Buhl, U., Arnon, S., Bar-Zeev, E., Oprei, A., Packman, A. I., Peralta-Maraver, I., Robertson,
801 A., Teitelbaum, Y., and Mutz, M.: Streambed migration frequency drives ecology and
802 biogeochemistry across spatial scales, Wiley Interdiscip. Rev.: Water, 10.
803 https://doi.org/10.1002/wat2.1632, 2023.

804 Rivett, M. O., Buss, S. R., Morgan, P., Smith, J. W. N., and Bemment, C. D.: Nitrate attenuation in
805 groundwater: A review of biogeochemical controlling processes, Water Res. 42, 4215–4232,
806 http://doi.org/10.1016/j.watres.2008.07.020, 2008.

807 Roche, K. R., Blois, G., Best, J. L., Christensen, K. T., Aubeneau, A. F., and Packman, A. I.:
808 Turbulence links momentum and solute exchange in coarse-grained streambeds, Water Resour.
809 Res. 54, 3225–3242, https://doi.org/10.1029/2017WR021992, 2018.

810 Roche, K. R., Li, A., Bolster, D., Wagner, G. J., and Packman, A. I.: Effects of turbulent hyporheic
811 mixing on reach-scale transport, Water Resour. Res. 55,
812 https://doi.org/10.1029/2018WR023421, 2019.

https://doi.org/10.5194/egusphere-2025-2631
Preprint. Discussion started: 29 July 2025

Rouse, J. D., Bishop, C. A., and Struger, J.: Nitrogen pollution: an assessment of its threat to amphibian survival, Environ. Health Perspect. 107, 799–803, https://doi.org/10.1289/ehp.99107799, 1999.

Santizo, K. Y., Widdowson, M. A., and Hester, E. T.: Abiotic mixing-dependent reaction in a laboratory simulated hyporheic zone, Water Resour. Res. 56 (9), e2020WR027090, https://doi.org/10.1029/2020WR027090, 2020.

Sawyer, A. H.: Enhanced removal of groundwater-borne nitrate in heterogeneous aquatic sediments, Geophys. Res. Lett. 42(2), 403–410, https://doi.org/10.1002/2014GL062234, 2015.

Schindler, R. J., Parsons, D. R., Ye, L., Hope, J. A., Baas, J. H., Peakall, J., Manning, A. J., Aspden, A. J., Malarkey, J., and Simmons, S.: Sticky stuff: redefining bedform prediction in modern and ancient environments, Geology, 43, 399–402, https://doi.org/10.1130/G36262.1, 2015.

Schulz, H., Teitelbaum, Y., Lewandowski, J., Singer, G. A., and Arnon, S.: Moving bedforms control CO2 production and distribution in sandy river sediments, J. Geophys. Res.: Biogeosci. 128, e2022JG007156, https://doi.org/10.1029/2022JG007156, 2023.

Shelley, F., Klaar, M., Krause, S., and Trimmer, M.: Enhanced hyporheic exchange flow around woody debris does not increase nitrate reduction in a sandy streambed, Biogeochem. 136 (3), 353-372, https://doi.org/10.1007/s10533-017-0401-2, 2017.

Song, X., Chen, X., Stegen, J., Hammond, G., Song, H.-S., Dai, H., Graham, E., and Zachara, J. M.: Drought conditions maximize the impact of high-frequency flow variations on thermal regimes and biogeochemical function in the hyporheic zone, Water Resour. Res. 54 (10), 7361–7382, https://doi.org/10.1029/2018WR022586, 2018.

https://doi.org/10.5194/egusphere-2025-2631
Preprint. Discussion started: 29 July 2025

834 Stelzer, R. S., and Bartsch, L. A.: Nitrate removal in deep sediments of a nitrogen-rich river network:
835 A test of a conceptual model, J. Geophys. Res. 117, G02027,
836 http://doi.org/10.1029/2012JG001990, 2012.

837 Teitelbaum, Y., Shimony, T., Cifuentes, E. S., Dallmann, J., Phillips, C. B., Packman, A. I., Hansen,
838 S. K., and Arnon, S.: A novel framework for simulating particle deposition with moving
839 bedforms, Geophys. Res. Lett. 49(4), e2021GL097223, https://doi.org/10.1029/2021GL097223,
840 2022.

841 Tonina, D., and Buffington, J. M.: Hyporheic exchange in gravel bed rivers with pool-riffle
842 morphology: Laboratory experiments and three-dimensional modeling, Water Resour. Res. 43,
843 W01421, https://doi.org/10.1029/2005WR004328, 2007.

844 Trauth, N., and Fleckenstein, J. H.: Single discharge events increase reactive efficiency of the
845 hyporheic zone, Water Resour. Res. 53(1), 779–798. https://doi.org/10.1002/2016WR019488,
846 2017.

847 Trauth, N., Musolff, A., Knller, K., Kaden, U. S., and Fleckenstein, J. H.: River water infiltration
848 enhances denitrification efficiency in riparian groundwater, Water Resour. 130, 185–199,
849 https://doi.org/10.1016/j.watres.2017.11.058, 2017.

850 Wolke, P., Teitelbaum, Y., Deng, C., Lewandowski, J., and Arnon, S.: Impact of bed form celerity on
851 oxygen dynamics in the hyporheic zone, Water, 12(1), 62, https://doi.org/10.3390/w12010062,
852 2019.

https://doi.org/10.5194/egusphere-2025-2631
Preprint. Discussion started: 29 July 2025

Wondzell, S. M., LaNier, J., Haggerty, R., Woodsmith, R. D., and Edwards, R. T.: Changes in hyporheic exchange flow following experimental wood removal in a small, low-gradient stream, Water Resour. Res. 45, https://doi.org/10.1029/2008WR007214, 2009.

Wu, L., Gomez-Velez, J. D., Li, L., and Carroll, K. C.: The fragility of bedform-induced hyporheic zones: Exploring impacts of dynamic groundwater table fluctuations, Water Resour. Res. 60, e2023WR036706, https://doi.org/10.1029/2023WR036706, 2024.

Xian, Y., Jin, M., Zhan, H., and Liang, X.: Permeable biofilms can support persistent hyporheic anoxic microzones, Geophys. Res. Lett. 49, e2021GL096948, https://doi.org/10.1029/2021GL096948, 2022.

Zarnetske, J. P., Haggerty, R., Wondzell, S. M., and Baker, M. A.: Dynamics of nitrate production and removal as a function of residence time in the hyporheic zone, J. Geophys. Res. Biogeosci. 116, G01025, https://doi.org/10.1029/2010JG001356, 2011a.

Zarnetske, J. P., Haggerty, R., Wondzell, S. M., and Baker, M. A.: Labile dissolved organic carbon supply limits hyporheic denitrification, J. Geophys. Res. Biogeosci. 116, G04036, https://doi.org/10.1029/2011JG001730, 2011b.

Zarnetske, J. P., Haggerty, R., Wondzell, S. M., Bokil, V. A., and González-Pinzón, R.: Coupled transport and reaction kinetics control the nitrate source-sink function of hyporheic zones, Water Resour. Res. 48 (11), 1–15, https://doi.org/10.1029/2012WR011894, 2012.

Zheng, L., Cardenas, M. B., Wang, L., and Mohrig, D.: Ripple effects: Bed form morphodynamics cascading into hyporheic zone biogeochemistry, Water Resour. Res. 55, 7320–7342, https://doi.org/10.1029/2018WR023517, 2019.

https://doi.org/10.5194/egusphere-2025-2631
Preprint. Discussion started: 29 July 2025

874 Zhu, Y., Dai, H., and Yuan, S.: The competition between heterotrophic denitrification and DNRA
875 pathways in hyporheic zone and its impact on the fate of nitrate, J. Hydrol. 626: 130175,
876 https://doi.org/10.1016/j.jhydrol.2023.130175, 2023.

877 Zomer, J. Y., and Hoitink, A. J. F.: Evidence of secondary bedform controls on river dune migration,
878 Geophys. Res. Lett. 51(15), https://doi.org/10.1029/2024GL109320, 2024.